Environmental Research 212 (2022) 113264

Contents lists available at ScienceDirect

Environmental Research

journal homepage: www.elsevier.com/locate/envres

A reusable and sensitive electrochemical sensor for determination of idarubicin in environmental and biological samples based on $NiFe_2O_4$ nanospheres anchored N-doped graphene quantum dots composite; an electrochemical and molecular docking investigation

Mohammad Mehmandoust [a], Pouran Pourhakkak [b], Gizem Tiris [c], Hassan Karimi-Maleh [d,e,f,*], Nevin Erk [a,**]

[a] Ankara University, Faculty of Pharmacy, Department of Analytical Chemistry, 06560, Ankara, Turkey
[b] Payame Noor University, Department of Chemistry, Tehran, Iran
[c] Bezmialem Vakif University, Faculty of Pharmacy, Department of Analytical Chemistry, 34093, Istanbul, Turkey
[d] School of Resources and Environment, University of Electronic Science and Technology of China, P.O. Box, 611731, Xiyuan Ave, Chengdu, PR China
[e] Department of Chemical Engineering, Quchan University of Technology, Quchan, Iran
[f] Department of Chemical Sciences, University of Johannesburg, Doornfontein Campus, 2028, Johannesburg, P.O. Box, 17011, South Africa

ARTICLE INFO

Keywords:
Idarubicin
Nickle ferrite
N-doped graphene quantum dots
Voltammetry
Docking investigation

ABSTRACT

An ultrasensitive and selective voltammetric sensor with ultra-trace level detection limit is introduced for idarubicin (IDA) determination in real samples. The as-synthesized nanocomposite was characterized by several techniques, including Fourier transform infrared spectroscopy (FT-IR), X-ray diffraction (XRD), Raman spectroscopy, Energy-dispersive X-ray spectroscopy (EDX), and Field emission scanning electron microscopy (FE-SEM). The electrocatalytic performance of the developed electrode was observed by cyclic voltammetry (CV), differential pulse voltammetry (DPV), electrochemical impedance spectroscopy (EIS), and chronoamperometry. The limit of detection (LOD) of the developed sensor for idarubicin is 1.0 nM, and the response is found to be in the dynamic concentration range of 0.01–1.9 μmol/L in a Britton–Robinson buffer (B-R, pH = 6.0). Moreover, the fabricated electrode illustrated high selectivity with good repeatability and reproducibility for diagnosing idarubicin as an anthracycline antileukemic drug. Furthermore, to evaluate the validity of the recommended method, three real samples, including human plasma, urine, and water samples, were analyzed with satisfactory recovery and compared with high-performance liquid chromatography (HPLC). The minor groove-binding mode of interaction was also supported by docking simulation studies, emphasizing that IDA can bind to ds-DNA preferably and confirmed experimental results. The reduced assay time and the possibility of measuring a single sample with another anticancer drug without any interference are significant advantages compared to the HPLC. The developed and validated sensor could be a valuable point-of-care diagnostic tool for IDA quantification in patients.

1. Introduction

Monitoring of pharmaceutical samples is so important strategy in medical investigations (ERK and Kartal, 1999; ERK and ONUR, 1997). Idarubicin (IDA), the most often used and effective anticancer medication, belongs to the anthracycline family of antibiotics having cytostatic action. Intercalation (squeezing between base pairs), DNA strand breaking, and suppression with the enzyme topoisomerase II are examples of IDA's general characteristics in contact with DNA (Karimi-Maleh et al., 2021). IDA is a structurally related cytotoxic antineoplastic antibiotic used to treat several forms of lymphoma, leukemia, sarcoma, and solid organ cancers. It is administrated as the oral

** Corresponding author.
* Corresponding author. School of Resources and Environment, University of Electronic Science and Technology of China, P.O. Box, 611731, Xiyuan Ave, Chengdu, PR China.
E-mail addresses: hassan@uestc.edu.cn (H. Karimi-Maleh), erk@pharmacy.ankara.edu.tr (N. Erk).

https://doi.org/10.1016/j.envres.2022.113264
Received 4 February 2022; Received in revised form 7 March 2022; Accepted 5 April 2022
Available online 12 April 2022

anthracycline antineoplastic, and the dosage and schedule are determined by the person's size and type of cancer. Like all other anticancer drugs, Vomiting, stomach pains, heart attack, and diarrhea are all possible adverse effects of IDA. As a result, it's critical to keep track of the amount of IDA in pharmaceutical formulations and blood samples. Researchers have used various methods to analyze IDA in real samples, demonstrating the breadth of its measurement. The approaches used are, including HPLC (Yang and Guo, 2002; Badea et al., 2005), fluorescence spectroscopy (Wei et al., 2016), ultraviolet–visible (UV-VIS) spectrophotometry (Hajian and Panahi, 2013; Ozluer and Kara, 2014), reverse-phase liquid chromatography (Eksborg and Nilsson, 1989; Kuhlmann et al., 1999), and phosphorescence (Ertas and Kara, 2015). Although the aforementioned methods demonstrate accurate results, they require expensive instrumentation and time-consuming sample pretreatment processes, increasing the cost and time of analysis, while electrochemical techniques based on fabricated sensors have several advantages, including a quick reaction time, simplicity, selectivity, and ease of miniaturization, making them desirable for routine analysis (Sohrabi et al., 2022; Roostaee and Sheikhshoaie, 2021; Tajik et al., 2021; Mehmandoust et al., 2021a, 2021b; Buledi et al., 2022). In electrochemical approaches, the most crucial parameters are to increase the active surface area and the reaction rate at a lower voltage of the electrode surface (Liu et al., 2021; Kannan and Maduraiveeran, 2022), which can be occurred by modifying the electrode surface with a conductive nanocomposite (Alavi-Tabari et al., 2018; Shabani-Nooshabadi and Roostaee, 2016; Shabani-Nooshabadi et al., 2017; Maheshwaran et al., 2021; Yamuna et al., 2021; Cheraghi et al., 2022; Ghalkhani et al., 2022; Lakhdari et al., 2021).

Nanomaterials with their unique properties and amazing properties have created a great revolution in various branches of science (Arefi-Oskoui et al., 2022; Keyikoglu et al., 2022; Taherian et al., 2021a, 2021b; Seid et al., 2022; Orooji et al., 2021). Due to high electrical conductivity, nanomaterials are good choice as catalyst for redox reactions(Alavi-Tabari et al., 2018; Orooji et al., 2022; Karaman, 2021; Gupta et al., 2015; Mohanraj et al., 2020). Nitrogen-doped graphene quantum dots (N-GQDs) are quasi-zero-dimensional nanomaterials with diameters less than 10 nm and doped with nitrogen atoms that are structurally formed of single-layer or multiple layers of graphene, can serve as an ideal electron mediate due to its edge effects, high conductivity, electrocatalytic activity, and biocompatibility (Mitchell et al., 2014; Kong et al., 2019; Yin et al., 2016). The N-GQDs exhibit more active sites in zero-dimensional materials due to their intrinsic properties, and because of these features, considerable research efforts have been studied using N-GQDs as modifier electrodes surface (Liang et al., 2021; Ju and Chen, 2015; Fu et al., 2019; Roushani and Shahdost-Fard, 2019). Therefore, N-GQDs' excellent characteristics can be used as an efficient platform in fabrication and sensing applications. When the N-GQDs are supported on materials, it demonstrates better electrochemical performance compared with unsupported N-GQDs (Silambarasan et al., 2021). Recently, the electrochemical properties of nickel ferrite ($NiFe_2O_4$) with spinel structures, which exhibits ferrimagnetism that originates from the magnetic moment of anti-parallel spins between Fe^{3+} ions at tetrahedral sites and Ni^{2+} ions at octahedral sites (Luo et al., 2010; Afkhami et al., 2014), have been investigated extensively due to their excellent electrical conductivity, the lower activation energy for electron transportation between cations, good structural stability, good biocompatibility, low toxicity, high adsorption ability, high effective surface area, and relatively higher specific capacitance (Ensafi et al., 2013; Yang et al., 2014; Ensafi and Allafchian, 2013). Decoration of graphene quantum dots with nickel ferrite nanospheres can enhance hybrid materials by imparting new optical, magnetic, and electrochemical properties. This is the first study of electrochemical IDA sensing in human plasma, urine, and water samples using N-GQDs@$NiFe_2O_4$/SPE to the best of our knowledge.

Considering the good characteristics in this work, we introduce a strategy employing N-GQDs@$NiFe_2O_4$ for selective IDA determination. Its unique three-dimensional structure of $NiFe_2O_4$ nanosphere endows excellent electrical conductivity and electrocatalytic activity, effectively enhancing the active surface area and loading many effective sites for the IDA determination. Under optimal conditions, good linearity was achieved using the DPV method. The IDA concentration was determined in the concentration range of 0.01–1.9 μM with a low LOD of 1.0 nM at pH 6.0 B-R buffer. Meanwhile, the N-GQDs@$NiFe_2O_4$ nanocomposites on the screen-printed electrode (N-GQDs@$NiFe_2O_4$/SPE) were employed for the real sample detection of IDA with satisfactory recovery. Under optimal experimental conditions, the influence of possible interferences and interactions between IDA and DNA was also examined.

2. Experimental

2.1. Materials and methods

The Supplementary Materials contained all the chemicals and equipment used for the experiment and comprehensive experimental instructions. Scheme 1 demonstrates the construction process of the N-GQDs@$NiFe_2O_4$/SPE and its use for IDA assay.

2.2. Molecular docking

Molecular docking is a noteworthy study to understand interactions between a ligand and a receptor, so it can be used to determine the ligand-DNA complex's binding mode (Ensafi et al., 2015). A molecular docking study was performed to forecast the binding mode of the IDA inside the DNA receptor. For this purpose, two DNA structures with d (CGCGAATTCGCG)2 and d(CGATCG)2 sequences were downloaded from Protein Data Bank (pdb:1BNA and pdb:1Z3F) to monitor the minor groove interactions and intercalation (http://www.pdb.org). The binding site of the dodecamer d(CGCGAATTCGCG)2 was recognized from the cavities within the structure of the DNA duplex with Discovery Studio 4.1. Two sites were discovered automatically, as shown in Fig. S1A. Small molecules have been declared to bind with DNA via minor grooves (Khan et al., 2012), so site1 was considered a binding site. Because the structure of DNA in 1Z3F is complexed with a ligand (ellipticine), the active site was calculated as a sphere with a radius of 9 around the bound ligand (Fig. S1B) to ensure that ligand and receptor sidechains within 9 of the binding site are free to move.

The DNA was produced using the CHARMm force field, with hydrogen atoms added and all water molecules removed. Discovery Studio 4.1 was also used to conduct a molecular docking investigation. To dock IDA into the DNA duplex, the GOLD software was used (Politi et al., 2010). GOLD is a genetic algorithm that accounts for the receptor's side-chain flexibility and considers flexible ligands. DrugBank (https://go.drugbank.com) was used to get the chemical structure of

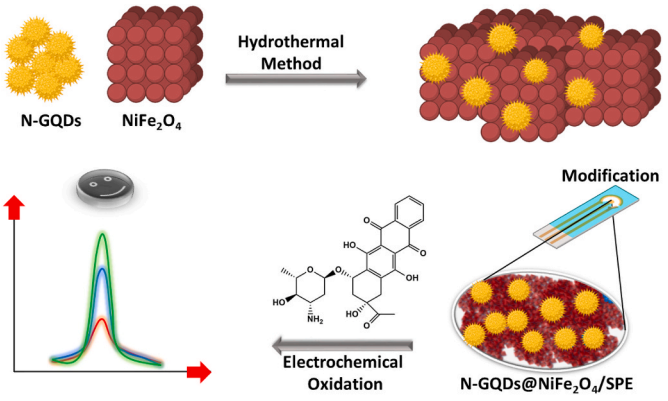

Scheme. 1. The construction processes of the N-GQDs@$NiFe_2O_4$/SPE electrochemical IDA sensor.

IDA, which was then imported into Discovery Studio. The CHARMm force field was then used to type it, and partial charges were calculated using the Momany-Rone option (Momany and Rone, 1992).

Afterward, it was reduced using 1000 steps of steepest descent Smart Minimization with an RMS gradient tolerance of 3 and conjugate gradient minimization. The default protocol settings were specified for the other parameters. Finally, a Gold score was utilized to assess the binding affinity of IDA toward the pocket of DNA. Root-mean-square distance (RMSD) value was estimated between bounded and re-docked ligand (ellipticine) to confirm the docking reliability. For this purpose, the original ligand was removed from DNA and docked into the binding site of DNA. The RMSD value of 0.9194 Å was achieved, showing the GOLD method's high reliability to reproduce the known binding mode. Fig. S2 shows the superimposition of the original (ellipticine) and re-docked ligand.

2.3. A commentary on the choice of materials

Herein, the best performance of IDA monitoring was studied using N-GQDs@$NiFe_2O_4$ on SPE. Due to their advantageous material properties, such as simplicity and rapid responses, screen-printed electrodes have been successfully utilized for quick in situ analysis. The $NiFe_2O_4$ and N-GQDs were selected to obtain a high-sensitive sensor for modifying SPE. $NiFe_2O_4$ is usually used as an electrode material for electrochemical sensors, owing to the large specific surface area, good electrical conductivity, and high specific capacitance (Jahani, 2018; Darabi and Shabani-Nooshabadi, 2021). The N-GQDs with high electrochemical activity enhance the sensor sensitivity (Li et al., 2017; Luo et al., 2020).

Moreover, because of π–π stacking interaction between N-GQDs and $NiFe_2O_4$, rise in electron mobility, and the delocalization of electrons on the whole composite N-GQDs@$NiFe_2O_4$ is preferred to sense an analyte. Therefore, to further improve the electrode's sensitivity and detection limit of IDA determination, N-GQDs@$NiFe_2O_4$ nanocomposite was used. Furthermore, $NiFe_2O_4$ was also used as a complementary modifying agent in electrode fabrication.

3. Results and discussion

3.1. Characterization of the N-GQDs@$NiFe_2O_4$ nanocomposite

FT-IR spectra for the crystalline N-GQDs@$NiFe_2O_4$ nanocomposite were investigated in the range of 4000–750 cm^{-1}, as shown in Fig. S1. The strong bands at 1375 (O–H bond bending) and 3444 cm^{-1} (stretching vibrations of H_2O absorbed by the sample) suggest the existence of hydroxyl functional groups (Ahmadian-Fard-Fini et al., 2019). Fig S3 also shows the band at 1100 and 1647 cm^{-1} corresponded to the C–O and C═O bonds, respectively, to the edges of GQDs during the oxidative cutting process (Chaturvedi et al., 2021).

XRD was also used to evaluate the structural identity and crystalline phase of the produced $NiFe_2O_4$ and N-GQDs@$NiFe_2O_4$ nanocomposite, as shown in Fig. 1A. Diffraction peaks with 2θ = 18.9°, 29.3°, 35.7°, 44.5°, 57.4°, and 60.1° are attributed to crystal planes of $NiFe_2O_4$. The XRD pattern of N-GQDs@$NiFe_2O_4$ nanocomposite retained the peaks of N-GQDs at around 2θ = 23.1 and 43.1, assigning to the (002) and (100) graphitic planes with d-spacings of 3.80 and 2.1 Å, respectively (Saisree et al., 2021). Comparing the XRD patterns of the $NiFe_2O_4$ and N-GQDs@$NiFe_2O_4$, It is evident that the intensity and location of the graphitic peaks for $NiFe_2O_4$ and N-GQDs@$NiFe_2O_4$ were almost identical, indicating the structure and crystallinity of $NiFe_2O_4$ were unaltered after the addition of N-GQDs, which is a confirmation of the successful synthesis of the nanocomposite. Fig. 1B shows the Raman spectra of $NiFe_2O_4$ and N-GQDs@$NiFe_2O_4$ and five first-order Raman active modes, attributed to $A_{1g}(1)$, $T_{2g}(3)$, $T_{2g}(2)$, E_g, and $T_{2g}(1)$, which are well consistent with the reported values of $NiFe_2O_4$ crystalline (Ahlawat et al., 2011; Selvadurai et al., 2015). Furthermore, the D and G bands were also found for N-GQDs@$NiFe_2O_4$ at 1385 and 1575 cm^{-1}, respectively, indicating the graphene structure in $NiFe_2O_4$@GQDs, where D band is several disorders in sp^2 hybridized carbon sheets and G band is graphitic carbon sp^2 of carbon atoms.

The morphology of the as-prepared $NiFe_2O_4$ and N-GQDs@$NiFe_2O_4$ was observed using SEM, as shown in Fig. 2. Fig. 2A and B shows that the spherical nanospheres of $NiFe_2O_4$ have an average size of 200 nm, increases the surface area against electro-catalytic oxidation. In the SEM image of N-GQDs@$NiFe_2O_4$ composite (Fig. 2C and D), GQDs have covered the entire surface of $NiFe_2O_4$, the sizes of N-GQDs@$NiFe_2O_4$ is in the range of 100–300 nm. The attained results of EDX are shown in Fig. S4 and Table S1. Peaks related to the presence of the elements of C, N, O, Fe, and Ni, accordingly confirming the synthesis of N-GQDs@$NiFe_2O_4$. The elemental mapping images of all elements clearly show that the N-GQDs@$NiFe_2O_4$ nanocomposite is a homogeneous distribution in Fig S5.

3.2. Electrochemical characterization of the N-GQDs@$NiFe_2O_4$/SPE

Fig. S6 illustrates the DPV of the bare SPE, $NiFe_2O_4$/SPE, and N-GQDs@$NiFe_2O_4$/SPE in 0.5 μM IDA containing 0.1 M B-R buffer solution at pH = 6.0. As shown in Fig. S6, a single oxidation peak was observed at 0.46 V for the N-GQDs@$NiFe_2O_4$/SPE, which attributes to the oxidation of IDA on the electrode surface. The oxidation current of IDA exhibits 2.4 times higher than bare SPE, which can be concluded that N-GQDs@$NiFe_2O_4$/SPE has excellent electroactive surface area and conductivity compared to a bare electrode and $NiFe_2O_4$/SPE. Moreover, the corresponding voltammetric curves illustrated that the modification of SPE surfaces by N-GQDs@$NiFe_2O_4$ composites astonishingly increased the IDA sensitivity with an excellent IDA electrocatalytic activity (i.e., from 495 to 460 mV) compared to that of bare SPE because of their active surface areas. The results confirm that there are synergic effects between N-GQDs and $NiFe_2O_4$.

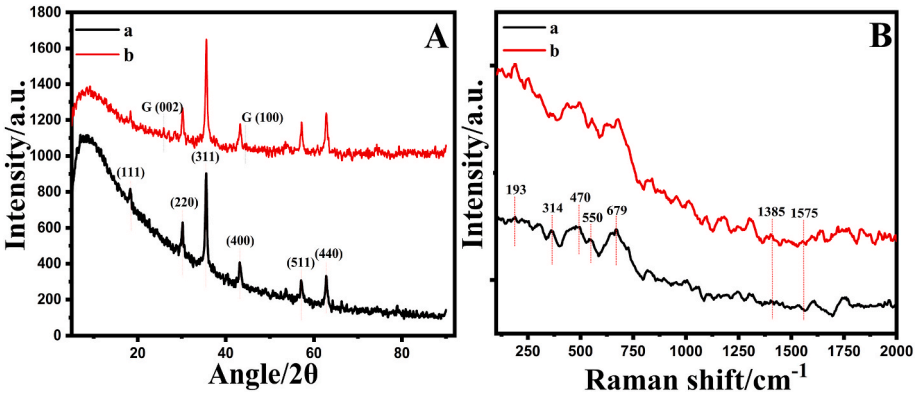

Fig. 1. (A); XRD patterns and (B); Raman spectra of $NiFe_2O_4$ (a) and N-GQDs@$NiFe_2O_4$ (b).

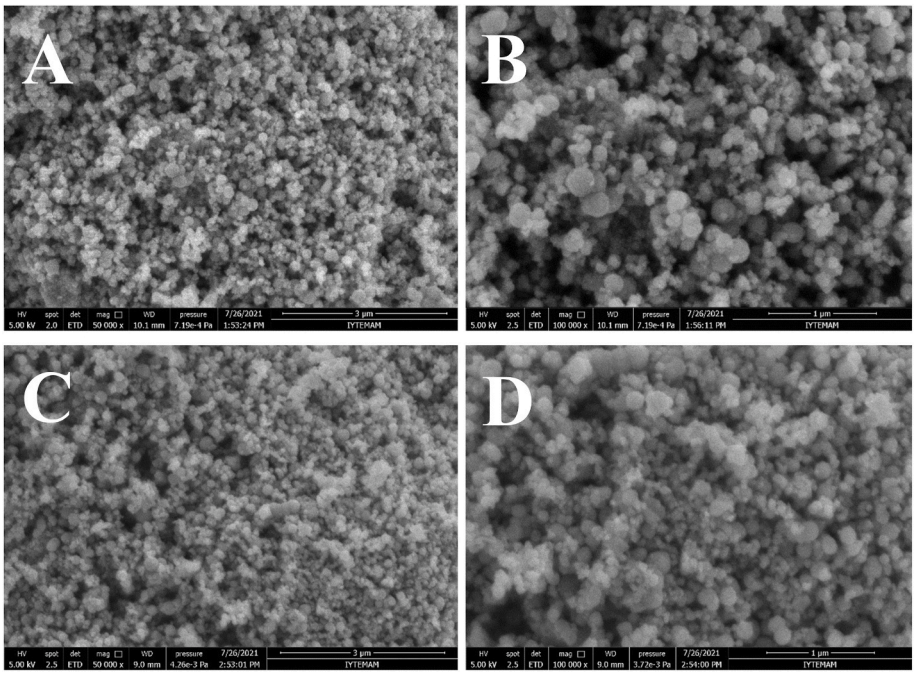

Fig. 2. SEM images of $NiFe_2O_4$ (A, B) and N-GQDs@$NiFe_2O_4$ (C, D).

Furthermore, CVs were utilized to study the electroanalytical performance of bare and developed electrodes in the absence of IDA. The results show that in the absence of analyte, the background current of N-GQDs@$NiFe_2O_4$ leads to enormous amounts compared to bare SPE and $NiFe_2O_4$/SPE (Fig. S7A) because of the tremendous electroactive surface area and good conductivity of the nanocomposite (Xie et al., 2013). In addition, the current density curves (Fig. S7B) confirm the more conductivity and active sites of mediators at a surface of N-GQDs@$NiFe_2O_4$/SPE.

The electrochemical characteristics of various electrodes were also studied by CV in $[Fe(CN)_6]^{3-/4-}$ as a standard redox solution. Fig. 3A exhibits the CV responses of bare SPE, $NiFe_2O_4$/SPE, and N-GQDs@$NiFe_2O_4$/SPE in 5.0 mM $[Fe(CN)_6]^{3-/4-}$ containing 0.1 M KCl. As shown, the highest peak current and the lowest potential separation were obtained on the N-GQDs@$NiFe_2O_4$/SPE compared to the bare electrode. Therefore, it could be concluded that the conductivity of the N-GQDs@$NiFe_2O_4$/SPE has increased (Alizadeh et al., 2021a, b), indicating an excellent electronic communication between composite and electrode due to the synergic effect of $NiFe_2O_4$ and GQDs on the electrode surface. A decreasing ΔEp value of N-GQDs@$NiFe_2O_4$/SPE indicates that the N-GQDs@$NiFe_2O_4$/SPE promotes electron transfer reactions. Moreover, the active surface area values of the bare electrode, $NiFe_2O_4$/SPE and N-GQDs@$NiFe_2O_4$/SPE were estimated by CVs using 5.0 mM $[Fe(CN)_6]^{3-/4-}$ containing KCl 0.1 M at different scan rates from 0.01 to 0.20 V s^{-1} using Randles–Sevcik formula (Mehmandoust et al., 2021) (Eq. S1).

From the slope of the plot of I_{pa} versus $\upsilon^{1/2}$, the electroactive surface area values of the bare electrode, $NiFe_2O_4$/SPE, and N-GQDs@$NiFe_2O_4$/SPE was calculated to be 0.21, 0.281, and 0.337 cm^2, indicating the active surface area of N-GQDs@$NiFe_2O_4$/SPE is approximately 2.5 times higher than the bare electrode. Furthermore, EIS was utilized to investigate electrode conductivity through the modification process within the frequency range of 0.1–10^5 Hz. Fig. 3B shows the Nyquist plots of bare SPE, $NiFe_2O_4$/SPE, and N-GQDs@$NiFe_2O_4$/SPE obtained in 5.0 mM $[Fe(CN)_6]^{3-/4-}$ containing 0.1 M KCl. As shown, a semicircle with a vast diameter (30.0 kΩ) is observed at the surface of the bare electrode. After modification of electrode by $NiFe_2O_4$ and N-GQDs@$NiFe_2O_4$/SPE, the charge transfer resistance (Rct) dramatically is decreased to 15.5 and 5.0 kΩ, respectively, indicating the presence of $NiFe_2O_4$ and N-GQDs at the electrode surface conduces a lowering of the electron transfer resistance, enhancing the electron transfer rate and conductivity, which could be attributed to the cooperative action between N-GQDs and $NiFe_2O_4$ that formed a high electron conduction pathway between the electrode and solution.

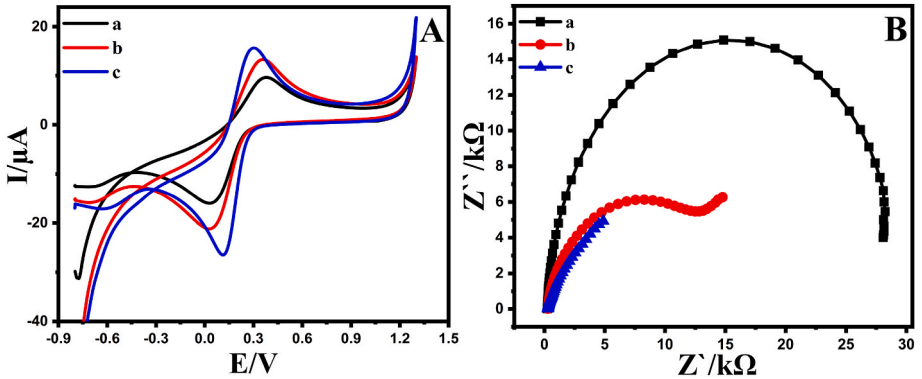

Fig. 3. (A); CV and (B); EIS of bare electrode (a), $NiFe_2O_4$/SPE (b) and N-GQDs@$NiFe_2O_4$/SPE in 5.0 mM $[Fe(CN)_6]^{3-/4-}$ containing 0.1 M KCl.

3.3. Optimization of experimental conditions

The amount and concentration of the N-GQDs@$NiFe_2O_4$/SPE nanocomposite at the electrode surface play an essential role in the electrocatalytic performance of the sensor (Butmee et al., 2019). It was observed that the oxidation peak of IDA gradually enhanced from 1.0 to 6.0 μL of the N-GQDs@$NiFe_2O_4$ suspension, and the maximum anodic current of IDA was observed at the amount 6.0 μL and concentration 1.0 mg mL^{-1}. This phenomenon discloses that N-GQDs@$NiFe_2O_4$ can remarkably increase the active surface area of the electrode surface, causing to higher accumulation of the IDA and increasing its oxidation. When the casted amount enhanced persistently, the peak current of the IDA did not considerably change. Therefore, 6.0 μL (1.0 mg mL^{-1}) of nanocomposite was utilized as optimum for the modification on the electrode surface. Furthermore, the effect of stirring and temperature of analyte was investigated and optimized at 150 rpm and 25 °C.

3.3.1. Effect of pH

The pH range of supporting electrolytes was observed from 2.0 to 10.0 in 0.5 μM IDA. The impact of pH on oxidation peak potential and the peak current is shown in Fig. 4A. Results exhibit that various pH affects the current response, and N-GQDs@$NiFe_2O_4$/SPE has the best electrocatalytic activity at pH 6.0, which was chosen for further experiments. Moreover, the peak current significantly reduced after pH 6.0 to 10.0. The electrostatic repulsion of anionic IDA with negative charges at the N-GQDs@NiFe2O4/SPE surface might explain the reduction in peak current at higher pH values. In addition, the plot of the E_{pa} against pH exhibits linearity on N-GQDs@$NiFe_2O_4$/SPE in the pH range from 2.0 to 10.0 with the following equations: E_{pa} = 0.9568–0.0732 pH (Fig. 4B). The slope value of the equation is near to the theoretical value of 0.0592 V/pH, showing that the transferred number of protons and electrons are equal for the oxidation process of IDA (Mehmandoust et al., 2021c). Therefore, the possible electro-oxidation mechanism for IDA at N-GQDs@$NiFe_2O_4$/SPE represents in Scheme 2, which causes the oxidation of the hydroxyl group to quinine. Results also exhibit that the reversible electron process leads to the formation of the quinolinic structure of IDA.

3.3.2. Effect of scan rate

The possible kinetic mechanism was observed further by cyclic voltammetry with various scan rates of 10.0–500.0 mV s^{-1} (Fig. 4C). The oxidation and reduction currents were enhanced linearly with the square root of scan rate in the range of 10.0–500.0 mV s^{-1} (Fig. 4D), showing the electrochemical oxidation of IDA at the N-GQDs@$NiFe_2O_4$/SPE was also a typical diffusion-controlled process. Moreover, as seen in Fig. 4C, N-GQDs@$NiFe_2O_4$/SPE exhibits the characteristic behavior, which is a shift in the oxidation and reduction peak potential with the

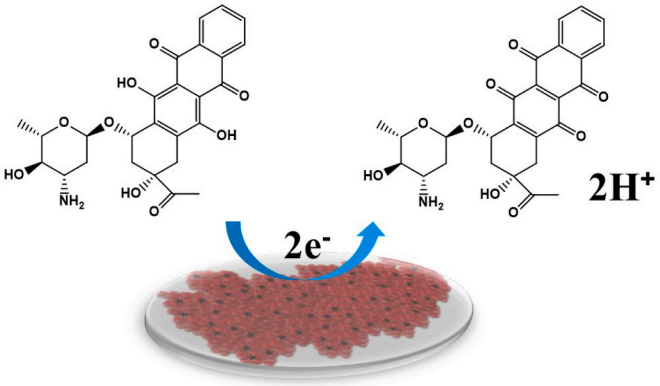

Scheme. 2. The possible mechanism of oxidation IDA at N-GQDs@$NiFe_2O_4$/SPE.

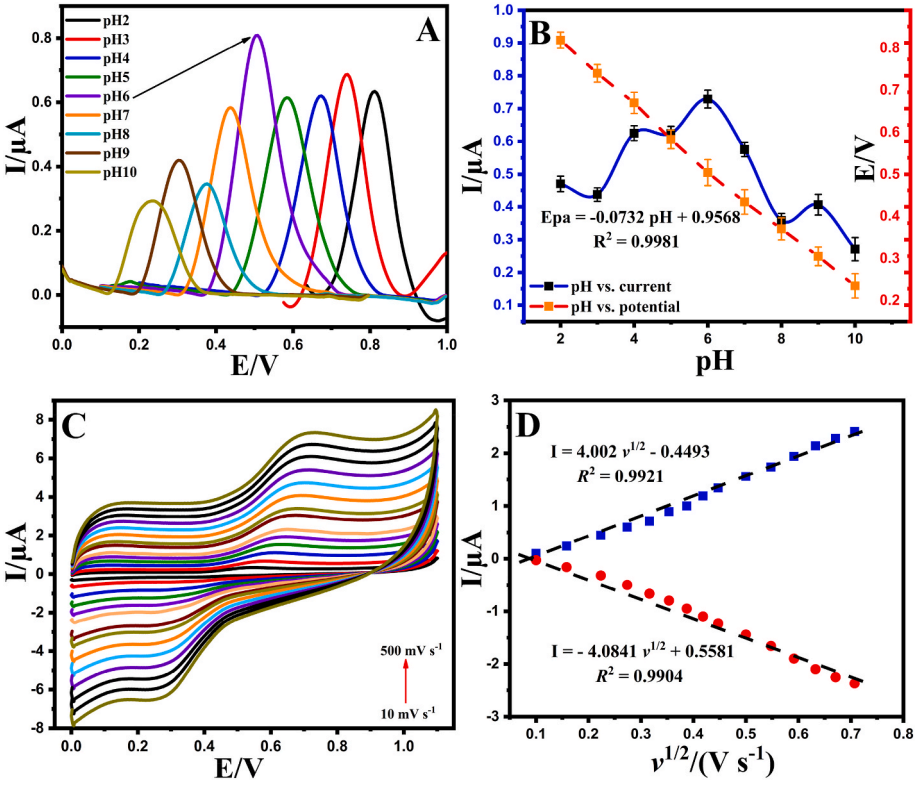

Fig. 4. (A); DPVs of 0.5 μM IDA in 0.1 M B-R buffer on N-GQDs@$NiFe_2O_4$/SPE surface at diverse pH (2.0–10.0), (B); Plot of E_{pa} and I_{pa} versus pH for IDA, (C); CVs of 0.5 μM IDA in 0.1 M B-R buffer at pH 6.0 on the surface of N-GQDs@$NiFe_2O_4$/SPE at diverse scan rates in the range of 10.0–500.0 mV s^{-1}, (D); Plots of the anodic and cathodic currents vs. square rate scan rates (n = 2).

enhancement of scan rate. Using the slope of Fig. S8, The number of the transferred electron could be calculated for a reversible and diffusion-controlled oxidation process using Laviron's theory (Eq. (1)).

$$Epa = E^0 + (\frac{RT}{\propto nF})ln(\frac{RTk^0}{\propto nF}) + (\frac{RT}{\propto nF})lnv \quad (1)$$

The number of transferred electrons for oxidation of IDA on the N-GQDs@$NiFe_2O_4$/SPE surface was estimated to be approximately ≈ 2 (n = 1.52), suggesting that two-electrons and two-protons are transferred during the oxidation step of IDA at the developed electrode surface (Scheme 2). The background current of IDA and the distortion in the form of the peak rise as scan speeds increase. If the scan rate is too slow, the current of the oxidation peak will decrease as the diffusion layer moves away from the electrode, resulting in a lower oxidation current toward the electrode (Faulkner and Bard, 2002). Therefore, an optimum scan rate of 50 mV/s was selected for further experiments.

3.4. Evaluation of kinetic parameter

The electrocatalytic oxidation of IDA was examined using a chronoamperometry technique to obtain the diffusion coefficient (D, cm^2 s^{-1}). By establishing the working electrode's voltage to 0.7 V, IDA chronoamprograms were detected at varying concentrations (400.0 and 600.0 μM) (Fig. S9). The diagrams of Ip in terms of $t^{-1/2}$ were then shown at various concentrations. The Cottrell equation (Eq. (2)) was used to calculate the diffusion coefficient of IDA:

$$I = nFAD^{\frac{1}{2}}C\pi^{\frac{-1}{2}}t^{\frac{-1}{2}} \quad (2)$$

where C is the IDA concentration (mol cm^{-3}), and A represents the electrode surface area (cm^2). The idarubicin D value was estimated to be 5.82×10^{-4} cm^2 s^{-1}.

3.5. Determination of IDA

DPV was used to quantitatively determine IDA after optimizing various parameters affecting the response peak current at N-GQDs@$NiFe_2O_4$/SPE. Fig. 5A exhibits the dependence of the DPV current on the concentration of IDA. A linear relation between signal and concentration was observed from 0.01 to 1.9 μM with a corresponding linear equation of I(μA) = 2.4081 C_{IDA}(μM) + 0.1154 (R^2 = 0.9955), as shown in Fig. 5B. Above 1.9 μM, the signal started to level off. Under the optimized analytical conditions, The limit of detection (LOD) was observed to be 1.0 nM (3σ/slope method, n = 10) (Baghayeri et al., 2019) with and high sensitivity (2.4081 μA $μM^{-1}$). Each point of the calibration was performed in triplicate, and the maximum relative standard deviation was less than 5.0%, which guaranteed the precision of the developed sensor.

3.6. Comparison of the sensor with previously reported IDA voltammetric sensors

We can infer that the developed sensor is comparable to the previously described IDA sensors based on published data for various electrode modifications (Table 1). The table demonstrates that our modified sensor has the best LOD for IDA determination so far. More interestingly, the modified sensor shows very high sensitivity for IDA compared to other sensors. Furthermore, N-GQDs are poorly investigated toward sensor development, and this article is one of few that deal with this research. It was also clear from Table 1 that the performance of N-GQDs@$NiFe_2O_4$/SPE is quite comparable or even better than the previously reported electrochemical sensors, indicating the ability of the N-GQDs@$NiFe_2O_4$/SPE towards sensitive determination of IDA.

3.7. Reproducibility, repeatability, stability, reusability

The reproducibility and repeatability of the as-fabricated sensor towards IDA determination were investigated. The relative standard deviation (RSD) of inter-electrode responses to 0.2 μM IDA at five different electrodes (reproducibility) was 2.77%, while the RSD of intra-electrode responses to repeated additions (ten times) of 0.2 μM IDA (repeatability) was observed to be 3.54%. Moreover, A modified electrode was chosen to detect IDA kept in the laboratory for 15 days to assess the stability and was measured in 0.2 μM IDA solution. The results exhibited that RSDs were 3.52%. Furthermore, the reusability of N-GQDs@$NiFe_2O_4$/SPE was observed. The results showed that N-GQDs@$NiFe_2O_4$/SPE is not a disposable sensor and can be regenerated via a simple room temperature DI water rinse (at least 10 times).

Table 1
Comparison of the N-GQDs@$NiFe_2O_4$/SPE with other modified electrodes.

Method	Electrode	Linear range (μM)	LOD (μM)	Ref.
DPV	Ru@VC/GCE[a]	0.05–1.0	0.009	Kaya et al. (2020)
DPV	MWCNT/GCE[b]	0.093–1.8	0.018	Kurbanoglu et al. (2013)
SWV[c]	TiO_2–CNF/CPE[d]	0.012–10.0	0.003	Arkan et al. (2017)
DPV	PC-rGO/MOF-199/CPE[e]	0.005–1.0	0.0015	Dehdashtian et al. (2019)
DPV	N-GQDs@$NiFe_2O_4$/SPE	0.01–1.9	0.001	Our work

[a] Ruthenium/Vulcan carbon-based nanomaterials on glassy carbon electrode.
[b] Multi wallet carbon nanotube on glassy carbon electrode.
[c] Square wave voltammetry.
[d] Titanium dioxide nanoparticles/carbon nanofibers on carbon paste electrode.
[e] Perlite/cobalt oxide/reduced graphene oxide/metal-organic framework composite on carbon paste electrode.

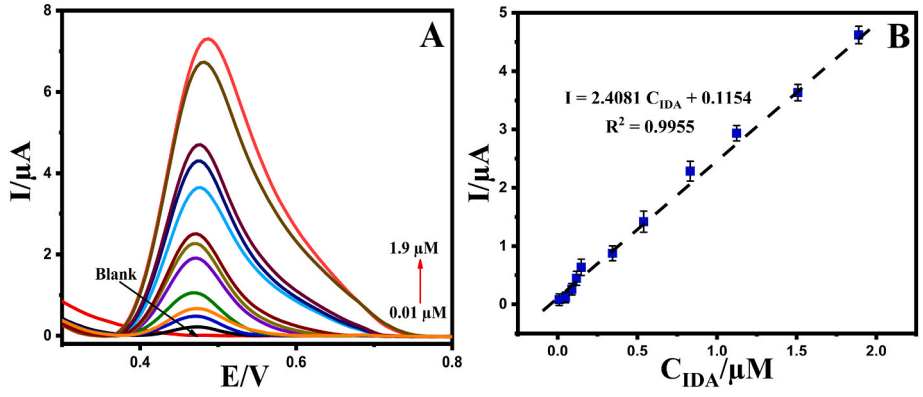

Fig. 5. (A); DPVs of N-GQDs@$NiFe_2O_4$/SPE in the presence of various IDA concentrations, (B); Plot of I_{pa} vs. IDA concentration at various concentrations (n = 3).

3.8. Interference study

To assess the as-fabricated sensor's selectivity, the fabricated electrode's ability towards the IDA determination in the presence of the various interferences was performed by DPV. The percentage change in the current signal in the presence of a 100-fold excess of dopamine (DP), ascorbic acid (AA), vitamin B (VB), vitamin D (VD), L-cysteine (CS), L-arginine (AG), L-glucose (GC), and uric acid (UA) was negligible interference effect in the determination of IDA (RSD<±5%), showing that N-GQDs@$NiFe_2O_4$/SPE has an outstanding selectivity towards IDA determination with prominent features. (Fig. S10).

3.8.1. Cross-reactivity

Idarubicin and mitomycin C are two quinone-containing anticancer drugs that are beneficial in treating several human cancers. Quinone-containing anticancer medicines can be bioreduced to reactive species by oxidoreductases, resulting in their cytotoxic effects. Therefore, the selectivity of the developed sensor was observed by measuring the response towards mitomycin C as possible interferent and then compared to the idarubicin sensor response. These results were represented as plots in Fig. S11. As can be seen, the DPV signals of mitomycin C and idarubicin are independent and not overlapped (RSD less than 6.0%).

On the other hand, the coexistence of mitomycin C in the electrolyte solution does not interfere with the signal of idarubicin and vice-versa, suggesting no cross-reactivity between them. Therefore, the N-GQDs@$NiFe_2O_4$/SPE can be successfully utilized for the IDA determination without any significant interference from compounds with a similar structure to IDA. This strategy can be applied in the case of real scenarios. This aspect is crucial because idarubicin is used mainly in binary combination with these drugs for therapeutic purposes.

3.9. Real sample analysis

To achieve an insight into the application of the N-GQDs@$NiFe_2O_4$/SPE as a reliable sensing alternative to determine the IDA level in real samples, the proposed sensor was utilized to detect IDA concentration in human plasma, urine, water samples provided, and the result obtained was listed in Table 2. The recovery for IDA was between 97.5% and 103.7%, and the RSD results were less than 5.0%, displaying that the fabricated sensor has acceptable sensitivity and accuracy in determining IDA in real samples and enormous potential in drug applications with satisfactory recovery. The analytical performance of a disposable N-GQDs@$NiFe_2O_4$/SPE was statistically compared to a validated HPLC (Kuhlmann et al., 1999) using Student's t-test and F-test. The corresponding values were lower than the tabulated values, indicating that the accuracy and precision of the proposed sensor are highly appropriate for analytical applications. However, HPLC techniques usually employ more expensive equipment and involve intricate and lengthy operations and the use of very hazardous organic solvents. Because of the general benefits of electroanalytical methods and the fact that it allows for easy and rapid measurements, the suggested approach for the IDA determination can be considered particularly desirable.

3.10. Interaction of IDA with DNA

The developed analytical method can be appropriate for exploring IDA and double-stranded DNA (dsDNA) interactions. DPVs of IDA in the absence and presence of DNA are presented in Scheme. S1. In the presence of IDA (20.0 and 40.0 μM), the oxidation potential of ds-DNA moved to a more positive position, and the oxidation current exhibited a considerable reduction, suggesting an intercalation reaction between IDA and guanine based on the ds-DNA structure and could be utilized as analytical parameters for the next stages. The results indicate that this developed sensor can be successfully determined in DNA, is appropriate for monitoring IDA concentration, and is valuable for medicinal relevance. Accordingly, this study offers the possibility of developing a DNA biosensor for detecting IDA.

3.10.1. Molecular docking in the minor groove

The idarubicin-dodecamer model revealed that IDA interacts with DNA via minor groove with a Gold score value of 24.8654 (Fig. 6). This scoring function considers factors such as H-bonding energy, van der Waals energy, and ligand torsion strain, in which a higher value is related to a higher affinity of binding. This value demonstrates the high affinity of IDA toward DNA. It can be seen from Fig. 6 that the hydrogen atoms of IDA functioned as donor moieties in the formation of O···H–O conventional hydrogen bonds (H-bond) and O···H–C carbon H-bonds with DT20 and DT7 base pairs, respectively. The oxygen atoms of the IDA drug act as H-bond acceptors and form 3 carbon H-bonds with DT7 base pairs. In addition, the methyl group of IDA can form 3 pi-alkyl hydrophobic interactions with DA5 and DA6.

3.10.2. Intercalation docking

Fig. 7 shows the best pose of the IDA-hexamer configuration with the Gold score value of 29.3105. This value affirms the high affinity of IDA toward DNA. It was discovered that the IDA drug intercalates into nitrogenous cytosine and guanine base pairs of the DNA. The IDA-DNA complex is stabilized by pi-alkyl and pi-sigma interactions and intermolecular H-bonds. An IDA's oxygen atom served as an acceptor moiety in forming an intermolecular O···H–N conventional H-bond with an H atom of deoxyguanosine 2 (DG2). Also, two hydrogen atoms of hydroxyl groups of IDA functioned as H-bond donor groups and interacted with DG2 and DG6 via conventional H-bonds. In addition, two Pi-sigma hydrophobic interactions occur between hydrogens of C–H moieties of IDA and base pairs' pi orbitals of DG6. Furthermore, methyl groups of IDA interact with the pi orbitals of DC1 and DG6 via pi-alkyl hydrophobic interactions. The resulting docking model revealed that the IDA drug

Table 2
IDA Determination in real samples by the developed method.

Sample	Added(μM)	Found[a](μM)	Recovery (%)[b]	RSD[c](%)	HPLC(μM)	Recovery(%)
Human plasma	0.4	0.39 ± 0.02	97.5	4.78	0.384 ± 0.003	104.1
	0.8	0.797 ± 0.05	99.6	1.32	0.823 ± 0.002	97.2
	1.0	1.01 ± 0.02	101.0	0.47	0.95 ± 0.02	94.6
	0.4	0.40 ± 0.03	100.0	4.28	–	–
Urine	0.8	0.83 ± 0.05	103.7	2.05	–	–
	1.0	1.01 ± 0.04	101.0	1.29	–	–
	0.4	0.38 ± 0.04	95.4	2.61	–	–
Water	0.8	0.8 ± 0.07	100.0	3.59	–	–
	1.0	0.95 ± 0.09	95.7	3.88	–	–
F-test	0.23	–	–	–	–	–
t-test	0.32	–	–	–	–	–

[a] Average of three replicate measurements.
[b] Recovery percentage = [Found/Added] × 100.
[c] Relative error = [(Proposed method − Comparative method)/(Comparative method)] × 100.

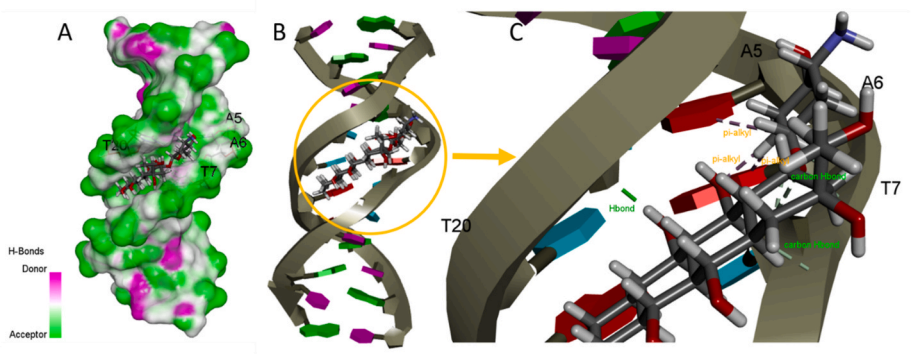

Fig. 6. The best docking pose of IDA in the minor groove of the duplex of dodecamer (1BNA) sequenced d(CGCGAATTCGCG)2, (A); Surface perspective of DNA colored by the H-bond ability of nucleotides, from violet for H-bond donor to green for H-bond acceptor, (B); the backbone of DNA and the base pairs represent in arrows and rings, respectively (color codes: deoxyadenosine (DA): red, deoxycytidine (DC): violet, deoxyguanosine (DG): green, deoxythymine (DT): blue), (C); H-bonds and hydrophobic interactions between IDA and DNA. (For interpretation of the references to color in this figure legend, the reader is referred to the Web version of this article.)

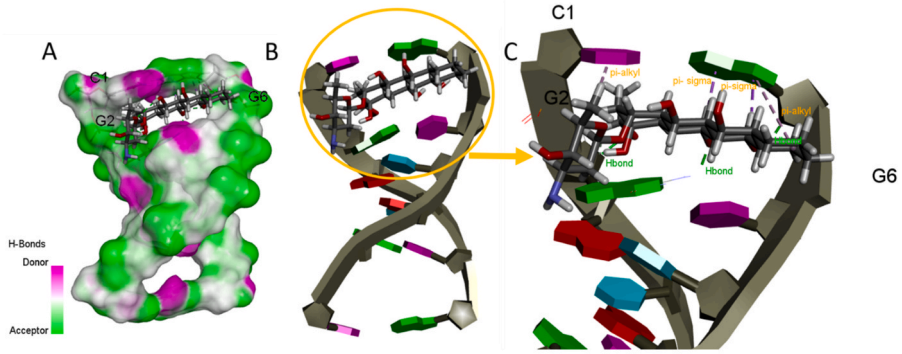

Fig. 7. (A) The surface view of idarubicin-hexamer docked complex, and (B) intercalation binding mode of IDA into DNA hexamer (1Z3F), (C) H-bonds, and hydrophobic interactions between IDA and DNA.

intercalates into the base pairs of DNA hexamer.

4. Conclusion

In summary, N-GQDs@$NiFe_2O_4$/SPE nanocomposite was introduced as a highly efficient electrocatalyst for IDA determination. Therefore, the developed electrode was used as a voltammetric sensor to determine IDA in real samples. The excellent capability of the N-GQDs@$NiFe_2O_4$/SPE to electrocatalytic oxidation of IDA was demonstrated using DPV experiments. The detection limit of the developed electrode for IDA was observed to be 1.0 nM with a linear range from 0.01 to 1.9 μM. The fabricated electrode demonstrated several advantages, including satisfying selectivity, stability, repeatability, and reproducibility. Moreover, DPV was conducted to determine the interactions of the IDA with ds-DNA. The changes in the electrochemical properties of IDA approved that IDA bind to DNA by electrostatic and groove binding modes. Furthermore, the Molecular docking study reaffirmed that IDA was a minor groove binder of ds-DNA. This study is valuable for a better understanding of IDA-DNA interaction, which should be imported into determining the therapeutic efficacy of the drug and the design of new DNA-targeted medicines in the future. Therefore, this developed approach is considered an excellent alternative for clinical analyses where the determination of trace levels of IDA is required.

Declaration of competing interest

The authors declare that they have no known competing financial interests or personal relationships that could have appeared to influence the work reported in this paper.

Acknowledgment

This work was supported by the Scientific Research Projects Commission of Ankara University (Project Number: 21B0237005 and 21H0237005).

Appendix A. Supplementary data

Supplementary data to this article can be found online at https://doi.org/10.1016/j.envres.2022.113264.

References

Afkhami, A., Khoshsafar, H., Bagheri, H., Madrakian, T., 2014. Preparation of NiFe2O4/graphene nanocomposite and its application as a modifier for the fabrication of an electrochemical sensor for the simultaneous determination of tramadol and acetaminophen. Anal. Chim. Acta 831, 50–59.

Ahlawat, A., Sathe, V., Reddy, V., Gupta, A., 2011. Mossbauer, Raman and X-ray diffraction studies of superparamagnetic NiFe2O4 nanoparticles prepared by sol–gel auto-combustion method. J. Magn. Magn Mater. 323, 2049–2054.

Ahmadian-Fard-Fini, S., Ghanbari, D., Salavati-Niasari, M., 2019. Photoluminescence carbon dot as a sensor for detecting of Pseudomonas aeruginosa bacteria: hydrothermal synthesis of magnetic hollow NiFe2O4-carbon dots nanocomposite material. Compos. B Eng. 161, 564–577.

Alavi-Tabari, S.A., Khalilzadeh, M.A., Karimi-Maleh, H., 2018. Simultaneous determination of doxorubicin and dasatinib as two breast anticancer drugs uses an amplified sensor with ionic liquid and ZnO nanoparticle. J. Electroanal. Chem. 811, 84–88.

M. Alizadeh, M. Mehmandoust, O. Nodrat, S. Salmanpour, N. Erk, A glassy carbon electrode modified based on molybdenum disulfide for determination of folic acid in the real samples, J. Food Meas. Char., 15(2021), 5622-5629. Alizadeh et al., 2021b Alizadeh, M., et al., 2021a. A glassy carbon electrode modified based on molybdenum disulfide for determination of folic acid in the real samples. J. Food Meas. Char. 15 (2021), 5622–5629.

Arefi-Oskoui, S., Khataee, A., Behrouz, S.J., Vatanpour, V., Gharamaleki, S.H., Orooji, Y., Safarpour, M., 2022. Development of MoS2/O-MWCNTs/PES blended membrane for efficient removal of dyes, antibiotic, and protein. Separ. Purif. Technol. 280, 119822.

Arkan, E., Paimard, G., Moradi, K., 2017. A novel electrochemical sensor based on electrospun TiO2 nanoparticles/carbon nanofibers for determination of Idarubicin in biological samples. J. Electroanal. Chem. 801, 480–487.
Badea, I., Lazăr, L., Moja, D., Nicolescu, D., Tudose, A., 2005. A HPLC method for the simultaneous determination of seven anthracyclines. J. Pharmaceut. Biomed. Anal. 39, 305–309.
Baghayeri, M., Nodehi, M., Veisi, H., Tehrani, M.B., Maleki, B., Mehmandost, M., 2019. The role of pramipexole functionalized MWCNTs to the fabrication of Pd nanoparticles modified GCE for electrochemical detection of dopamine. Daru 27, 593–603.
Buledi, J.A., Mahar, N., Mallah, A., Solangi, A.R., Palabiyik, I.M., Qambrani, N., Karimi, F., Vasseghian, Y., Karimi-Maleh, H., 2022. Electrochemical quantification of mancozeb through tungsten oxide/reduced graphene oxide nanocomposite: a potential method for environmental remediation. Food Chem. Toxicol. 161, 112843.
Butmee, P., Tumcharern, G., Saejueng, P., Stankovic, D., Ortner, A., Jitcharoen, J., Kalcher, K., Samphao, A., 2019. A direct and sensitive electrochemical sensing platform based on ionic liquid functionalized graphene nanoplatelets for the detection of bisphenol A. J. Electroanal. Chem. 833, 370–379.
Chaturvedi, A.K., Pappu, A., Srivastava, A.K., Gupta, M.K., 2021. Synthesis dielectric and mechanical properties of paddy straw derived graphene quantum dots-stone waste nanocomposite. Mater. Lett. 301, 130323.
Cheraghi, S., Taher, M.A., Karimi-Maleh, H., Karimi, F., Shabani-Nooshabadi, M., Alizadeh, M., Al-Othman, A., Erk, N., Raman, P.K.Y., Karaman, C., 2022. Novel enzymatic graphene oxide based biosensor for the detection of glutathione in biological body fluids. Chemosphere 287, 132187.
Darabi, R., Shabani-Nooshabadi, M., 2021. NiFe2O4-rGO/ionic liquid modified carbon paste electrode: an amplified electrochemical sensitive sensor for determination of Sunset Yellow in the presence of Tartrazine and Allura Red. Food Chem. 339, 127841.
Dehdashtian, S., Hashemi, B., Aeenmehr, A., 2019. The application of perlite/cobalt oxide/reduced graphene oxide (PC-rGO)/metal organic framework (MOF) composite as electrode modifier for direct sensing of anticancer drug idarubicin. IEEE Sensor. J. 19, 11739–11745.
Eksborg, S., Nilsson, B., 1989. Reversed-phase liquid chromatographic determination of idarubicin and its 13-hydroxy metabolite in human plasma. J. Chromatogr. B Biomed. Sci. Appl. 488, 427–434.
Ensafi, A.A., Allafchian, A.R., 2013. Multiwall carbon nanotubes decorated with NiFe2O4 magnetic nanoparticles, a new catalyst for voltammetric determination of cefixime. Colloids Surf. B Biointerfaces 102, 687–693.
Ensafi, A.A., Jafari-Asl, M., Rezaei, B., Allafchian, A., 2013. Simultaneous determination of guanine and adenine in DNA based on NiFe2O4 magnetic nanoparticles decorated MWCNTs as a novel electrochemical sensor using adsorptive stripping voltammetry. Sensor. Actuator. B Chem. 177, 634–642.
Ensafi, A.A., Heydari-Soureshjani, E., Jafari-Asl, M., Rezaei, B., Ghasemi, J.B., Aghaee, E., 2015. Experimental and theoretical investigation effect of flavonols antioxidants on DNA damage. Anal. Chim. Acta 887, 82–91.
ERK, N., Kartal, M., 1999. Comparison of High-Performance Liquid Chromatography and Absorbance Ratio Methods for the Determination of Hydrochlorothiazide and Lisinopril in Pharmaceutical Formulations.
ERK, N., ONUR, F., 1997. Three new spectrophotometric methods for simultaneous determination of hydrochlorothiazide and amiloride hydrochloride in sugar-coated tablets. Anal. Lett. 30, 1503–1515.
Ertas, N., Kara, H.E.S., 2015. l-Cysteine capped Mn-doped ZnS quantum dots as a room temperature phosphorescence sensor for in-vitro binding assay of idarubicin and DNA. Biosens. Bioelectron. 70, 345–350.
Faulkner, L.R., Bard, A.J., 2002. Electrochemical Methods: Fundamentals and Applications. John Wiley and.
Fu, Y., Gao, G., Zhi, J., 2019. Electrochemical synthesis of multicolor fluorescent N-doped graphene quantum dots as a ferric ion sensor and their application in bioimaging. J. Mater. Chem. B 7, 1494–1502.
Ghalkhani, M., Zare, N., Karimi, F., Karaman, C., Alizadeh, M., Vasseghian, Y., 2022. Recent advances in Ponceau dyes monitoring as food colorant substances by electrochemical sensors and developed procedures for their removal from real samples. Food Chem. Toxicol. 112830.
Gupta, V.K., Karimi-Maleh, H., Sadegh, R., 2015. Simultaneous determination of hydroxylamine, phenol and sulfite in water and waste water samples using a voltammetric nanosensor. Int. J. Electrochem. Sci. 10, 303–316.
Hajian, R., Panahi, F., 2013. Spectroscopic and Electrochemical Monitoring on the Binding of Idarubicin as a Chemotherapy Drug with Ds-. DNA.
Jahani, S., 2018. Evaluation of the usefulness of an electrochemical sensor in detecting ascorbic acid using a graphite screen-printed electrode modified with NiFe2O4 nanoparticles. Anal Bioanal Electrochem 10, 739–750.
Ju, J., Chen, W., 2015. In situ growth of surfactant-free gold nanoparticles on nitrogen-doped graphene quantum dots for electrochemical detection of hydrogen peroxide in biological environments. Anal. Chem. 87, 1903–1910.
Kannan, P., Maduraiveeran, G., 2022. Bimetallic nanomaterials-based electrochemical biosensor platforms for clinical applications. Micromachines 13, 76.
Karaman, C., 2021. Orange peel derived-nitrogen and sulfur Co-doped carbon dots: a nano-booster for enhancing ORR electrocatalytic performance of 3D graphene networks. Electroanalysis 33, 1356–1369.
Karimi-Maleh, H., Khataee, A., Karimi, F., Baghayeri, M., Fu, L., Rouhi, J., Karaman, C., Karaman, O., Boukherroub, R., 2021. A green and sensitive guanine-based DNA biosensor for idarubicin anticancer monitoring in biological samples: a simple and fast strategy for control of health quality in chemotherapy procedure confirmed by docking investigation. Chemosphere 291, 132928.
Kaya, S.I., Kurbanoglu, S., Yavuz, E., Mustafov, S.D., Sen, F., Ozkan, S.A., 2020. Carbon-based ruthenium nanomaterial-based electroanalytical sensors for the detection of anticancer drug Idarubicin. Sci. Rep. 10, 1–12.
Keyikoglu, R., Khataee, A., Lin, H., Orooji, Y., 2022. Vanadium (V)-doped ZnFe LDH for enhanced sonocatalytic degradation of pymetrozine. Chem. Eng. J. 134730.
Khan, G.S., Shah, A., Barker, D., 2012. Chemistry of DNA minor groove binding agents. J. Photochem. Photobiol. B Biol. 115, 105–118.
Kong, F.-Y., Yao, L., Li, R.-F., Li, H.-Y., Wang, Z.-X., Lv, W.-X., Wang, W., 2019. Synthesis of nitrogen-doped reduced graphene oxide loading with Au-Ag bimetallic nanoparticles for electrochemical detection of daunorubicin. J. Alloys Compd. 797, 413–420.
Kuhlmann, O., Hofmann, S., Weiss, M., 1999. Determination of idarubicin and idarubicinol in rat plasma using reversed-phase high-performance liquid chromatography and fluorescence detection. J. Chromatogr. B Biomed. Sci. Appl. 728, 279–282.
Kurbanoglu, S., Dogan-Topal, B., Uslu, B., Can, A., Ozkan, S.A., 2013. Electrochemical investigations of the anticancer drug idarubicin using multiwalled carbon nanotubes modified glassy carbon and pyrolytic graphite electrodes. Electroanalysis 25, 1473–1482.
Lakhdari, D., Guittoum, A., Benbrahim, N., Belgherbi, O., Berkani, M., Vasseghian, Y., Lakhdari, N., 2021. A novel non-enzymatic glucose sensor based on NiFe (NPs)–polyaniline hybrid materials. Food Chem. Toxicol. 151, 112099.
Li, L., Liu, D., Wang, K., Mao, H., You, T., 2017. Quantitative detection of nitrite with N-doped graphene quantum dots decorated N-doped carbon nanofibers composite-based electrochemical sensor. Sensor. Actuator. B Chem. 252, 17–23.
Liang, A.A., Hou, B.H., Tang, C.S., Sun, D.L., Luo, E.A., 2021. An advanced molecularly imprinted electrochemical sensor for the highly sensitive and selective detection and determination of Human IgG. Bioelectrochemistry 137, 107671.
Liu, J.-G., Wan, J.-Z., Lin, Q.-M., Han, G.-C., Feng, X.-Z., Chen, Z., 2021. Convenient heme nanorod modified electrode for quercetin sensing by two common electrochemical methods. Micromachines 12, 1519.
Luo, L., Li, Q., Xu, Y., Ding, Y., Wang, X., Deng, D., Xu, Y., 2010. Amperometric glucose biosensor based on NiFe2O4 nanoparticles and chitosan. Sensor. Actuator. B Chem. 145, 293–298.
Luo, L., Liu, X., Ma, S., Li, L., You, T., 2020. Quantification of zearalenone in mildewing cereal crops using an innovative photoelectrochemical aptamer sensing strategy based on ZnO-NGQDs composites. Food Chem. 322, 126778.
Maheshwaran, S., Akilarasan, M., Chen, T.-W., Chen, S.-M., Tamilalagan, E., Jiang, T.-Y., Alabdullkarem, E.A., Soylak, M., 2021. Electrocatalytic evaluation of graphene oxide warped tetragonal t-lanthanum vanadate (GO@ LaVO4) nanocomposites for the voltammetric detection of antifungal and antiprotozoal drug (clioquinol). Microchim. Acta 188, 1–9.
Mehmandoust, M., Erk, N., Karaman, O., Karimi, F., Bijad, M., Karaman, C., 2021a. Three-dimensional porous reduced graphene oxide decorated with carbon quantum dots and platinum nanoparticles for highly selective determination of azo dye compound tartrazine. Food Chem. Toxicol. 112698.
Mehmandoust, M., Erk, N., Alizadeh, M., Salmanpour, S., 2021. Voltammetric carbon nanotubes based sensor for determination of tryptophan in the milk sample. J. Food Meas. Char. 5288–5295.
Mehmandoust, M., Erk, N., Karaman, C., Karaman, O., 2021b. An electrochemical molecularly imprinted sensor based on CuBi2O4/rGO@ MoS2 nanocomposite and its utilization for highly selective and sensitive for linagliptin assay. Chemosphere 132807.
Mehmandoust, M., Çakar, S., Özacar, M., Salmanpour, S., Erk, N., 2021c. Electrochemical sensor for facile and highly selective determination of antineoplastic agent in real samples using glassy carbon electrode modified by 2D-MoS2 NFs/TiO2 NPs. Top. Catal. 1–13.
Mitchell, B., Siobhan, J., Thomas, N., 2014. Graphene quantum dots. Part. Part. Syst. Char. 31, 415–428.
Mohanraj, J., Durgalakshmi, D., Rakkesh, R.A., Balakumar, S., Rajendran, S., Karimi-Maleh, H., 2020. Facile synthesis of paper based graphene electrodes for point of care devices: a double stranded DNA (dsDNA) biosensor. J. Colloid Interface Sci. 566, 463–472.
Momany, F.A., Rone, R., 1992. Validation of the general purpose QUANTA® 3.2/CHARMm® force field. J. Comput. Chem. 13, 888–900.
Orooji, Y., Tanhaei, B., Ayati, A., Tabrizi, S.H., Alizadeh, M., Bamoharram, F.F., Karimi, F., Salmanpour, S., Rouhi, J., Afshar, S., 2021. Heterogeneous UV-Switchable Au nanoparticles decorated tungstophosphoric acid/TiO2 for efficient photocatalytic degradation process. Chemosphere 281, 130795.
Orooji, Y., Nezafat, Z., Nasrollahzadeh, M., Shafiei, N., Afsari, M., Pakzad, K., Razmjou, A., 2022. Recent advances in nanomaterial development for lithium ion-sieving technologies. Desalination 529, 115624.
Ozluer, C., Kara, H.E.S., 2014. In vitro DNA binding studies of anticancer drug idarubicin using spectroscopic techniques. J. Photochem. Photobiol. B Biol. 138, 36–42.
Politi, A., Durdagi, S., Moutevelis-Minakakis, P., Kokotos, G., Mavromoustakos, T., 2010. Development of accurate binding affinity predictions of novel renin inhibitors through molecular docking studies. J. Mol. Graph. Model. 29, 425–435.
Roostaee, M., Sheikhshoaie, I., 2021. A novel, sensitive and selective nanosensor based on graphene nanoribbon–cobalt ferrite nanocomposite and 1-methyl-3-butylimidazolium bromide for detection of vanillin in real food samples. J. Food Meas. Char. 1–10.
Roushani, M., Shahdost-Fard, F., 2019. Applicability of AuNPs@ N-GQDs nanocomposite in the modeling of the amplified electrochemical Ibuprofen aptasensing assay by monitoring of riboflavin. Bioelectrochemistry 126, 38–47.

Saisree, S., Aswathi, R., Nair, J.A., Sandhya, K., 2021. Radical sensitivity and selectivity in the electrochemical sensing of cadmium ions in water by polyaniline-derived nitrogen-doped graphene quantum dots. New J. Chem. 45, 110–122.
Seid, L., Lakhdari, D., Berkani, M., Belgherbi, O., Chouder, D., Vasseghian, Y., Lakhdari, N., 2022. High-efficiency electrochemical degradation of phenol in aqueous solutions using Ni-PPy and Cu-PPy composite materials. J. Hazard Mater. 423, 126986.
Selvadurai, A.P.B., Pazhanivelu, V., Murugaraj, R., 2015. A phenomenal behaviour of nanocrystalline NiFe 2 O 4: influence of secondary and parasitic phases on structure and magnetic property. Appl. Phys. A 119, 299–307.
Shabani-Nooshabadi, M., Roostaee, M., 2016. Modification of carbon paste electrode with NiO/graphene oxide nanocomposite and ionic liquids for fabrication of high sensitive voltammetric sensor on sulfamethoxazole analysis. J. Mol. Liq. 220, 329–333.
Shabani-Nooshabadi, M., Roostaee, M., Karimi-Maleh, H., 2017. Incorporation of graphene oxide–NiO nanocomposite and n-hexyl-3-methylimidazolium hexafluoro phosphate into carbon paste electrode: application as an electrochemical sensor for simultaneous determination of benserazide, levodopa and tryptophan. J. Iran. Chem. Soc. 14, 955–961.
Silambarasan, K., Harish, S., Hara, K., Archana, J., Navaneethan, M., 2021. Ultrathin layered MoS2 and N-doped graphene quantum dots (N-GQDs) anchored reduced graphene oxide (rGO) nanocomposite-based counter electrode for dye-sensitized solar cells. Carbon 181, 107–117.
Sohrabi, H., Majidi, M.R., Arbabzadeh, O., Khaaki, P., Pourmohammad, S., Khataee, A., Orooji, Y., 2022. Recent advances in the highly sensitive determination of zearalenone residues in water and environmental resources with electrochemical biosensors. Environ. Res. 204, 112082.
Taherian, Z., Khataee, A., Han, N., Orooji, Y., 2021a. Hydrogen production through methane reforming processes using promoted-Ni/mesoporous silica: a review. J. Ind. Eng. Chem.
Taherian, Z., Gharahshiran, V.S., Khataee, A., Orooji, Y., 2021b. Synergistic effect of freeze-drying and promoters on the catalytic performance of Ni/MgAl layered double hydroxide. Fuel 122620.
Tajik, S., Lohrasbi-Nejad, A., Mohammadzadeh Jahani, P., Askari, M.B., Salarizadeh, P., Beitollahi, H., 2021. Co-detection of carmoisine and tartrazine by carbon paste electrode modified with ionic liquid and MoO3/WO3 nanocomposite. J. Food Meas. Char. 1–9.
Wei, X., Huang, X., Fang, Y., Zhang, Q., 2016. Determination of idarubicin using CdTe quantum dots as fluorescence probes. J. Nanosci. Nanotechnol. 16, 6992–6997.
Xie, L., Xu, Y., Cao, X., 2013. Hydrogen peroxide biosensor based on hemoglobin immobilized at graphene, flower-like zinc oxide, and gold nanoparticles nanocomposite modified glassy carbon electrode. Colloids Surf. B Biointerfaces 107, 245–250.
Yamuna, A., Hong, C.-Y., Chen, S.-M., Chen, T.-W., Alabdullkarem, E.A., Soylak, M., AL-Anazy, M.M., Ali, M.A., Liu, X., 2021. Highly selective simultaneous electrochemical detection of trace level of heavy metals in water samples based on the single-crystalline Co3O4 nanocubes modified electrode. J. Electroanal. Chem. 887, 115159.
Yang, M.-c., Guo, Z.-f., 2002. Study on HPLC determination of idarubicin hydrochloride and related substances. CHINESE PHARMACEUTICAL JOURNAL-BEIJING- 37, 945–947.
Yang, W., Gao, Z., Ma, J., Zhang, X., Wang, J., Liu, J., 2014. Hierarchical NiCo 2 O 4@ NiO core–shell hetero-structured nanowire arrays on carbon cloth for a high-performance flexible all-solid-state electrochemical capacitor. J. Mater. Chem. 2, 1448–1457.
Yin, Y., Liu, Q., Jiang, D., Du, X., Qian, J., Mao, H., Wang, K., 2016. Atmospheric pressure synthesis of nitrogen doped graphene quantum dots for fabrication of BiOBr nanohybrids with enhanced visible-light photoactivity and photostability. Carbon 96, 1157–1165.